Proton SEU Cross Sections Derived from Heavy-Ion Test Data

Larry D. Edmonds
Jet Propulsion Laboratory*
California Institute of Technology
Mail Stop 303-220
4800 Oak Grove Drive
Pasadena, California 91109-8099
Phone: (818) 354-2778
FAX: (818) 393-4559

Abstract

Many papers have presented models for estimating proton SEU cross sections from heavy-ion test data, but all rigorous treatments to date are based on the sensitive volume (SV) model for charge collection. Computer simulations have already shown that, excluding devices utilizing physical boundaries for isolation, there is no well-defined SV. A more versatile description of charge collection, which includes the SV model as a special case, utilizes a charge-collection efficiency function that measures the effect that the location of ionization has on collected charge. This paper presents the first rigorous analysis that uses a generic charge-collection efficiency function to relate proton to heavy-ion cross sections. The most practical result is an upper bound for proton SEU or SEL cross sections, which requires no information about the charge-collection efficiency function, except that it exists. In addition, some models previously presented by others are reproduced (or, in one case, extended) by applying the general theory to special cases. The similarities and differences between a variety of models become clear when the models are recognized to be special cases or variations of this general theory.

* The research in this paper was carried out by the Jet Propulsion Laboratory, California Institute of Technology, under contract with the National Aeronautics and Space Administration, Code AE, under the NASA Microelectronics Space Radiation Effects Program (MSREP).

I. INTRODUCTION

Many semiconductor devices flown in space are exposed to both heavy ions from galactic cosmic rays (in addition to other possible sources) and a large proton flux from solar events and/or a planetary radiation belt. Regarding single event effects (SEE), the most important types of reactions induced in a device can be different for the two particle types (direct ionization from heavy ions, versus the creation of reaction products by protons via nuclear reactions, with the reaction products producing the ionization). Therefore the most reliable SEE rate calculations utilize experimentally measured device proton cross sections for proton SEE rates, and utilize experimentally measured heavy-ion cross sections for heavy-ion SEE rates. Heavy-ion tests are typically considered to be essential for devices that will be exposed to heavy ions, because it is very risky to deduce heavy-ion cross sections from proton test data (as pointed out later in Section VIII). Therefore, a very common situation in practice is that in which a device has been tested with heavy ions but not yet tested with protons. A proton test is an additional expense, so there is a motivation to derive models that predict proton cross sections from heavy-ion test data. This is the subject of the present paper. The analysis is intended for a certain class of SEE in which the physical postulates in Section II are believed to be adequate approximations. Single event upset (SEU) is the prototype assumed in most of the discussions, but the analysis is expected to also apply to single event latchup (SEL). The results derived here are limited to those cases in which direct ionization from protons is not important, so the proton cross section is entirely due to reaction products created by the protons.

Many papers have derived relationships between proton and heavy-ion SEU susceptibility. However, all rigorous treatments (i.e., the physical postulates are precisely stated, and rigorous analysis is applied to the postulates) to date use the sensitive volume (SV) model as the physical postulate. This model states that the portion of the charge liberated by an ionizing particle that contributes to SEU is the charge liberated within some definite volume within the device. Charge liberated outside the volume is assumed to make no contribution. However, computer simulations show that, excluding devices

utilizing physical boundaries for isolation, there is no such volume. Instead, charge collected at a device node changes continuously as the source of ionization (e.g., an ion track) is moved. A more realistic description of charge collection recognizes that charge liberated at any location (within limits established by physical boundaries) makes some contribution to collected charge, but the amount depends on the source location. A physical postulate that is more versatile than the SV model (but includes the SV model as a special case) is that there is a charge-collection efficiency function (a function of the spatial coordinates within a device) that measures the effect of source location on collected charge. The analysis given here is the first rigorous analysis that explicitly includes a charge collection efficiency function to derive a correlation between heavy-ion and proton SEU or SEL cross sections.

The analysis leads to several conclusions. The conclusion having the most practical applications (because it does not require information that is not available), is an upper bound for proton cross sections. Additional conclusions are equalities (instead of inequalities or bounds) derived for each of several special cases. These additional conclusions may become useful if future work finds ways to obtain the required information, but another motivation for presenting them is academic curiosity. It is interesting to see the similarities and differences between various cases. It is also interesting to compare these conclusions to results previously derived by other investigators.

In spite of limitations of the SV model, nearly all of the numerous published papers that predict proton cross sections from heavy-ion data report good agreement between measured proton cross sections and model predictions. However, previous results generally contain adjustable parameters selected for a good track record, in the sense of producing agreement for the majority of the cases in which comparisons were made between measurement and predictions. Even after a good track record has been established, there is still some uncertainty as to whether a new case of interest will conform to the same pattern. This uncertainty is a risk to a flight project that is relying on model predictions for a particular device that has not been tested with protons. The upper

bound presented in Section III contains no arbitrary or adjustable parameters, hence there is no artificial way to obtain a good track record. A disadvantage is that the upper bound can sometimes be excessively conservative, particularly for devices that are completely immune to protons. The only required input information is heavy-ion test data (from long-range, normal-incident ions), which is not enough information to determine proton cross sections, so the upper bound is a more accurate proton cross section estimate for some devices than for others. The upper bound is the proton cross section for the worst possible device (i.e., having the greatest possible proton susceptibility) consistent with the heavy ion test data. However, it will be seen in Section VI that this "worst" device is not always a rare or hypothetical case. It is fairly common for real devices that are susceptible to protons to be nearly this bad, in the sense that the proton cross sections are within a factor of three of this upper bound.

II. PHYSICAL POSTULATES

A. The First Postulate

The first physical postulate assumes that for each point **x** in a device, there is a weighting function $\Omega(\mathbf{x})$ which measures the relative importance of an increment of charge (e.g., a piece of an ion track) liberated at the point **x**, compared to the same amount of charge liberated at other locations. To be more specific, suppose two points in the device $\mathbf{x}_1$ and $\mathbf{x}_2$ satisfy $\Omega(\mathbf{x}_1)=2\Omega(\mathbf{x}_2)$. Then a given amount of charge liberated near the point $\mathbf{x}_1$ will produce the same device response as twice this charge liberated near the point $\mathbf{x}_2$. The precise and complete statement of the first postulate is that there exists a function Ω and a constant Q_c (a property of the device) such that

$$\textit{SEE occurs if and only if} \quad \int \rho(\bar{x})\,\Omega(\bar{x})\,d^3x > Q_c \tag{1}$$

where ρ is the excess charge density (charge per unit volume) liberated by a particle hit, and the volume integral integrates over the entire device. For SEU, the relevant physical quantity is charge collected at a device node. In this case, Q_c is the critical charge and Ω can be called a charge-collection efficiency function. For the special case of the SV

model, Ω equals 1 inside the SV and zero outside. Note that if the relevant physical quantity is charge collected over a finite time period associated with some device time constant, then Q_c is the critical value of charge collected over this time period, and Ω is the weighting function for this quantity. The first postulate is quite general. For example, Q_c could be a time integral of the product of some current (possibly at a device contact, but not necessarily), multiplied by some coefficient that favors current at early times more than current at later times (with "early" and "late" defined by some device time constant). Whatever the physical quantity is that Q_c represents, Ω is the weighting function for that quantity. The upper bound estimate given in Section III does not require that we even know what kind of physical quantity (e.g., charge collected at a device contact, or something else) that Q_c and Ω refer to. The only requirement is that some constant Q_c and some corresponding function Ω satisfying (1) *exist* (we do not have to know what they are). Because of this generality, the theory is expected to apply to SEL as well as to SEU. However, in order to use familiar terminology, the prototype assumed for most discussions is SEU. We will call Q_c the critical charge, and we will call Ω the charge-collection efficiency function.

B. The Second Postulate

The second postulate is probably the weakest part of the analysis, and future work may find ways to improve upon this. This postulate is presently needed to simplify the analysis. This postulate assumes that reaction products created by protons have short enough ranges so that Ω can be approximated as a constant over the reaction product trajectory.

The second postulate has one tendency to produce conservative proton cross section estimates. The worst possible proton reaction allowed by the second postulate is that in which all charge liberated by the reaction products is liberated at a point where Ω is maximum, i.e., all liberated charge is collected with the maximum efficiency. In reality, if Ω varies considerably over a reaction product trajectory, then contributions to the liberated charge from different source locations cannot all be collected with the

maximum efficiency. Unfortunately, there is another tendency to underestimate proton cross sections. The explanation is simplest for the SV model, so we assume that this model applies for the purpose of illustration. The second postulate does not recognize reactions outside the SV that send reaction products into the SV. In reality this can occur, so the actual proton SEU cross section can include some events in which reactions occur outside the SV, while the calculated cross section excludes such events.

The second postulate is a crude approximation for a real device, but it may not be as bad as the SV model would indicate. To discuss this, we first discuss two types of depths in a device. The most familiar of the two depths is the *charge-collection* depth, defined to be collected charge from a long- (effectively infinite) range normal-incident ion, divided by the charge per unit length liberated along the ion track. The charge-collection depth defined this way is a variable (a function of the lateral coordinates describing the ion hit location), as previously noted by Barak *et al.* [1] when discussing the cross section associated with the charge-collection depth exceeding a specified value. The first physical postulate stated above implies that the charge-collection depth at a given lateral location is the integral of Ω along a perpendicular line through the device at that lateral location. Another depth, the *contributing* depth, is the depth at which Ω is small enough to be neglected at greater depths. It is only for the SV model that the charge-collection depth and contributing depth are equal. More generally (assuming that Ω does not exceed 1 anywhere in the device), the contributing depth is larger than the charge-collection depth.

The second physical postulate requires that reaction product ranges (at least for those reaction products that are most important to the device proton cross section) be less than the contributing depth, but this can be more lenient than requiring the ranges to be less than the charge-collection depth. For a hypothetical illustration, suppose that at some lateral location we have Ω=0.1 within a 10 μm depth, and Ω=0 below this depth. The charge-collection depth at this lateral location is only 1 μm, but the contributing depth is 10 μm, and the second postulate provides a fairly good approximation when the reaction product ranges are only a few microns. This hypothetical example is probably not very

typical, so it does not furnish a convincing argument that the second postulate is a good approximation. The approximation may still be crude, and improving upon this might be a worthwhile objective. The intention of this example is merely to argue that the approximation might be a little better than the SV model would suggest.

III. AN UPPER BOUND FOR PROTON SEU CROSS SECTIONS

It is easy to show that the postulates in Section II imply that the SEU proton cross section $\sigma_{pr}(E)$, for protons having energy E, can be expressed as

$$\sigma_{pr}(E) = n\int \alpha(E, \frac{Q_c}{\Omega(\vec{x})})\, d^3x \tag{2}$$

where n is the density of targets (number of silicon atoms per unit volume) and $\alpha(E,Q)$ is the per target cross section for a proton having energy E to produce a reaction that liberates a charge exceeding Q. Note that the integrand in (2) is zero at any location where $\Omega=0$, so the volume integral in (2) can be taken to be over the entire device (in fact, it can be over all space). It is shown in the appendix that the first postulate implies that the cross section $\sigma_{hi}(L)$, for long-range heavy ions having LET L, satisfies

$$\int_0^\infty \frac{1}{L}\frac{d\sigma_{hi}(L)}{dL}\, dL = \frac{a}{Q_c}\int \Omega(\vec{x})\, d^3x \tag{3}$$

where

$$a = 1.04\times 10^{-10}\, \frac{coul}{cm}\, [MeV - cm^2/mg]^{-1}$$

is a unit conversion factor for converting LET into liberated charge per unit length along the ion track.

Now define $\beta(E)$ by

$$\beta(E) \equiv \max_Q [Q\, n\, \alpha(E,Q)]. \tag{4}$$

Note that (4) implies

$$Q\, n\, \alpha(E,Q) \le \beta(E)$$

or

$$n\, \alpha(E,Q) \le \frac{\beta(E)}{Q}$$

so (2) gives

$$\sigma_{pr}(E) \le \frac{\beta(E)}{Q_c} \int \Omega(\vec{x})\, d^3x$$

and using (3) produces the upper bound

$$\sigma_{pr}(E) \le \frac{\beta(E)}{a} \int_0^\infty \frac{1}{L} \frac{d\sigma_{hi}(L)}{dL}\, dL\,. \tag{5}$$

IV. EVALUATION OF β

To calculate β from (4), we need to evaluate nα. The nα(E,Q) used here is the same as the BGR(E,E_r) function used by Normand (Fig.1 in [2]), but with a unit conversion applied so that nα(E,Q) is expressed as a function of liberated charge Q instead of the energy E_r deposited by the reaction products. Note that these data apply to neutrons, which is a good approximation for protons only at the larger values of E (>100 MeV). This should be adequate for practical applications, because the proton saturation cross section (i.e., large E cross section) is the most important parameter for proton-induced SEU rates in typical space environments. This is because a typical proton environment shielded by typical spacecraft shielding is such that most protons having energies large enough to create SEUs, also have energies large enough for the cross section to be roughly equal to the saturation cross section. Therefore, the shape of the σ_{pr}(E) versus E curve at small E is only of secondary importance for SEU rate calculations. Also, Barak *et al.* provided an efficiency factor that can be used for refining SEU rate estimates derived from the saturation cross section (Table 1 in [3]).

A fairly good fit to the data when E ≥ 50 MeV has the form

$$n\alpha(E,Q) = A(E)\, e^{-B(E)Q} \tag{6}$$

which gives

$$\beta(E) = \frac{A(E)}{B(E)\, e}$$

where A, B, and β are given in Table 1 below

E (MeV)	A(E) (1/cm)	B(E) (1/pC)	β(E) (coul-μm^2/cm^3)
50	0.030	23.099	4.78×10^{-8}
100	0.022	14.433	5.61×10^{-8}
200	0.020	9.935	7.41×10^{-8}

Table 1: Fitting parameters A and B for nα, and the implied β

V. NUMERICAL ALGORITHMS

The upper bound proton cross section is given by (5). There are several ways to evaluate the integral in (5). One way is a numerical integration. Another way applies to those cases (which are common but not universal) in which the heavy-ion cross section can be adequately fit by an analytic function having a known integral. A third method is also a numerical integration, but it utilizes an existing computer code that calculates heavy-ion SEU rates in a user-supplied environment. The second two methods are discussed separately below.

A. Evaluation via an Exponential Fit

A simple function that frequently (not always) produces a good fit to heavy-ion SEU or SEL cross section data is given by

$$\sigma_{hi}(L) = \sigma_0 \exp(-\frac{L_{1/e}}{L}) \tag{7}$$

where σ_0 (a constant) is the saturation cross section, and $L_{1/e}$ (a constant) is the LET value at which the cross section is 1/e times the saturation cross section. Although (7) was derived from physical analysis [4], it does not apply to all cases. One reason (perhaps not the only reason) is that a sum of functions of the type given by (7) is not another function of the same type, unless $L_{1/e}$ is the same for all terms in the sum. Therefore (7) does not apply to devices containing dissimilar components that contribute to the cross section. However, (7) is worth considering, because it frequently does apply, and a test for determining whether it does apply is very simple. The test plots the cross section against 1/L on semi-logarithmic paper (the cross section uses the logarithmic scale), and (subject to qualifications in the next paragraph) we look for a straight line.

Two considerations are relevant when testing the applicability of (7). The first involves cosine-law errors. Heavy-ion tests typically change the tilt angle of the device relative to the ion beam to mimic a change in ion LET, and the data are then converted via an assumed cosine law. The converted data are intended to represent the device susceptibility at normal incidence. However, the cosine-law conversion is only an approximation, and not always a good approximation. An unfortunate property of the popular Weibull function is that it fits a certain class of cosine-law errors (those giving the illusion of a fast approach to saturation) very well. This is unfortunate because cosine-law errors are not always noticed. The fit given by (7) generally does not fit cosine-law errors, so preference should be given to data measured at normal incidence when determining whether the fit applies.

The second consideration is that (7) has no threshold LET (the LET at which the cross section is zero). This is not a concern as long as the cross section calculated from (7) is negligibly small at LET less than the experimentally measured threshold LET. The straight line previously discussed often fails to fit the smallest LET (largest 1/LET) data, but this is usually not an important concern.

An example is provided by data obtained by Levinson *et al.* [5] for the HM65162 SRAM produced in 1985 (the year is relevant because there are different versions of the

device having different SEL cross sections). Measured heavy-ion cross section data (points), and a fit (curve) obtained from (7) are shown in Fig.1. The fitting parameters are σ_0=0.116 cm^2, $L_{1/e}$=28.3 MeV-cm^2/mg. It is not known which, if any, of the points might contain cosine-law errors (i.e., were measured at angles), so the fit attempted to accommodate all points. The seemingly low cross section at the largest LET data point might be influenced by a recombination loss discussed by Levinson *et al.* [5], so this point was given a low priority when selecting the fit. Note that the calculated cross section is negligible for LET below that of the lowest LET point, even though (7) has no threshold LET.

For those devices such the (7) provides an adequate approximation, the integral in (5) can be evaluated, and the result is

$$\sigma_{pr}(E) \le \frac{\beta(E)}{a}\frac{\sigma_0}{L_{1/e}} \quad (\textit{equivalent to } (5) \textit{ when } (7) \textit{ applies}). \tag{8}$$

B. Evaluation via a Heavy-Ion Rate Calculation

This method performs a numerical integration by using an existing computer code that calculates heavy-ion SEU rates in a user-supplied environment. The physics assumed by the code must be consistent with the first postulate in Section II, but this includes the SV model, which is used in the standard codes. This is a convenient method for individuals accustomed to calculating heavy-ion SEU rates, because no programming is required, and routine calculations can be used. To use such a code for this application, note that (3) applies not only to cross sections measured at normal incidence, but also to cross sections measured at any angle, if σ_{hi} is interpreted as the directional cross section. Therefore

$$\left[\int_0^\infty \frac{1}{L}\frac{d\sigma_{hi}(L)}{dL}\,dL\right]_{normal\ incidence} = \left[\int_0^\infty \frac{1}{L}\frac{d\sigma_{hi}(L)}{dL}\,dL\right]_{any\ angle}.$$

The solid angle integral of the above equation produces a heavy-ion SEU rate in an isotropic environment (with the integral LET flux proportional to 1/L) on the right side. The result is

$$\frac{1}{a}\int_0^{\infty}\frac{1}{L}\frac{d\sigma_{hi}(L)}{dL}\,dL = r^*\left[day-cm^2\,\frac{cm^3}{coul-\mu m^2}\right] \qquad (9)$$

where r* is defined by

r* ≡ Heavy-ion rate for a device having a normal-incident cross section σ_{hi} and produced by an integral LET flux H* given by H*(L)=(0.8856/m^2-sec-ster)(MeV-cm^2/mg)/L.

The constant in the flux H* was selected so that inconvenient constants do not appear in (9). The flux H* will be called the hypothetical 1/L flux. Substituting (9) into (5) gives

$$\sigma_{pr}\#(E) \le \beta\#(E)\; r^*\#\quad (\textit{equivalent to}\ (5)) \qquad (10)$$

where the quantities in (10) are the dimensionless numbers defined by

$$\sigma_{pr}\#(E) \equiv \sigma_{pr}(E)/cm^2$$
$$\beta\#(E) \equiv \beta(E)/[coul\text{-}\mu m^2/cm^3]$$
$$r^*\# \equiv r^*/[1/day].$$

In other words, σ_{pr}#(E) is the numerical part of σ_{pr}(E) when expressed in the units of cm^2. Analogous statements apply to the other quantities.

Note that r* would not be well defined if the flux was other than the hypothetical 1/L flux, because a normal-incident cross section would not otherwise uniquely determine the heavy-ion SEU rate. Different devices can have the same normal-incident data but different directional cross sections at other angles. This difference will produce different SEU rates in most heavy-ion environments. However, (9) implies that, for this special and hypothetical heavy-ion environment, different devices having the same normal-incident data also have the same heavy-ion SEU rate, even though they may have different directional cross sections at other angles.

Readers that would like to see a demonstration of the above assertion can do so by using a standard computer code that calculates the heavy-ion SEU rate for the traditional rectangular parallelepiped (RPP) shaped SV. All RPPs being compared are given the same upper surface areas and threshold LETs, so that they have the same normal-incident cross section curve, but they are given different thicknesses (with correspondingly

different critical charges so that the threshold LETs are the same). In most environments, the calculated rate for each RPP will depend on the RPP thickness. However, for the hypothetical 1/L flux, the same rate will be calculated for all choices of the RPP thickness (except for numerical errors, e.g., associated with data interpolation/extrapolation and/or approximations for chord-length distribution functions).

Any computer code consistent with the first postulate in Section II should calculate the same value for r*. Note, however, that the conventional model used for smooth device cross section curves is the integral RPP (IRPP) model [6], which regards a device as a collection of RPPs, that may have different critical charges. This model does not satisfy the first postulate in Section II, because different values of Q_c are associated with different RPPs. However, each RPP satisfies the postulate, so (5), (9), and (10) apply to the individual RPPs. Summing these results over the RPPs produces the same results (5), (9), and (10) but with the cross sections interpreted as device cross sections. We can therefore use these results together with the traditional IRPP method for calculating r* (the RPP thickness is arbitrary because the same r* is calculated for any thickness).

Most existing computer codes that can be used to calculate r* accept the environment in the form of a table of heavy-ion flux versus LET. If the code allows the user to select the LET values appearing in the table, we must consider both numerical errors from coarseness of the tabulation, and whether the code will have to extrapolate outside the range of the table (keeping in mind that thin RPPs require the flux to be evaluated at LETs much less than the threshold LET). Based on these considerations, a suggested tabulation is

$$L_i\# = 10^{(\frac{i}{25}-3)}, \quad H_i^*\# = \frac{0.8856}{L_i\#} \quad for\ i = 0,1,...,175 \tag{11a}$$

where

$$L_i\# \equiv L_i/[\text{MeV-cm}^2/\text{mg}]$$
$$H_i^*\# \equiv H_i^*/[1/\text{m}^2\text{-sec-ster}].$$

If the computer code accepts the environment in the form of a differential (in LET) flux h* instead of an integral flux H*, a suggested tabulation is

$$L_i\# = 10^{(\frac{i}{25}-3)}, \quad h_i^*\# = \frac{0.8856}{L_i\#^2} \quad for\ i = 0,1,...,175 \tag{11b}$$

where

$$h_i^*\# \equiv h_i^*/[(1/m^2\text{-sec-ster})/(MeV\text{-}cm^2/mg)].$$

The numerical algorithm for calculating an upper bound for the proton cross section via the rate calculation method is summarized as follows. A standard computer code designed to calculate heavy-ion SEU rates in a user supplied isotropic environment is used. The environment given to the code is either the integral flux H* or the differential flux h* (as dictated by the computer code), which can be tabulated as indicated in (11). The code is also given the device heavy-ion cross section data, and the code calculates the heavy-ion SEU rate r*. If the code uses the IRPP method, the RPP thickness is arbitrary (the same r* will be calculated from any thickness) as long as the thickness is not extreme enough to create large numerical errors. The upper bound estimate is then obtained from (10), with β obtained from Table 1.

C. The Relevant LET Range

A property of the integral in (5) that may seem unfortunate is that significant contributions to the integral can come from the high-LET portion of the σ_{hi} curve; from LETs larger than we might expect to be relevant to proton cross sections. Three reasons for this are:

(a) A conservative property of the second physical postulate (Section II) tends to exaggerate the importance of the high-LET portion of the σ_{hi} curve.

(b) Intentional conservatism that makes the estimate for σ_{pr} an upper bound can sometimes exaggerate the importance of the high-LET portion of the σ_{hi} curve.

(c) Some contribution to σ_{pr} from the higher-LET portions of the σ_{hi} curve is *real*. This was pointed out be Petersen [7]. Furthermore, the experimentally measured σ_{pr} can sometimes be under-estimated by not integrating to large enough LET, again indicating that some contribution to σ_{pr} from the higher-LET portions of the σ_{hi} curve is real.

It is not always clear how much of the high-LET contribution to σ_{pr} is an exaggeration and how much of it is real. Therefore the upper bound estimate for σ_{pr} cannot be considered to be a reliable upper bound unless the integration includes all LETs that significantly contribute to the integral in (5). This generally means integrating to near saturation of the σ_{hi} curve. One way to do this is to use the exponential fit for σ_{hi} together with (8), which includes all contributions from the complete curve. Another way is to use a Weibull fit for σ_{hi} together with the rate calculation method. A good computer code that calculates heavy-ion rates from Weibull parameters will include all relevant LETs.

A problem is most likely when no fit is used and many points are read directly from the σ_{hi} plot. This is tedious, so it is tempting to exclude the higher-LET points. Devices having threshold LETs greater than 12 MeV-cm^2/mg are often assumed to be immune to protons, so it is tempting to ignore the portion of the σ_{hi} curve having L>12. An example in which this is inadequate is furnished by the AMD K-5 microprocessor. Heavy-ion SEL data (from internal JPL memos) are plotted in Fig.2. The two highest points are very crude estimates, because the SEL rate was large enough to overwhelm the instrumentation at these points. The points were not fit, so the curve in the figure is a hand sketch. If the portion of the curve having L>12 is ignored, the upper bound for σ_{pr} calculated from (10) for E=200 MeV is only 1.1×10^{-9} cm^2. The measured value is 5.6×10^{-9} cm^2, so the intended upper bound actually underestimated the cross section. However, if the entire plotted range of the curve is included, the calculated upper bound becomes 1.9×10^{-8} cm^2.

D. MBUs

Devices soft enough to be susceptible to protons are often also susceptible to multiple-bit-upsets (MBUs) from heavy ions (sometimes also protons), i.e., one particle hit upsets several bits or cells. Several types of device cross sections can be defined. One type, called the U-type here (U for upset), is calculated from the total number of upsets observed during an SEU test, while another type, called the G-type here (G for group), counts the number of occurrences of upset groups. An upset group is defined here to be the set of upsets (one or more) produced by the same particle hit. For example, if one particle hit upsets four cells, the U-type cross section counts this as four upsets, while the G-type counts this as one group. The G-type is useful when one upset group is regarded as one device failure, regardless of whether the group contains one or many cell upsets. There are also variations of the G-type, e.g., the G3-type, which counts the number of occurrences of groups containing three upsets. The G-type device cross section is the sum in n of the Gn-type cross sections, while the U-type is the sum in n of n times the Gn-type. Only the U-type device cross section has the property of being the sum of the bit or cell cross sections. The U-type device cross section can be larger than the area of the entire device, because cell cross sections can overlap to the extent that the sum of these cross sections is larger than the device area. If all cells in the device are identical, the cell (or bit) cross section is the U-type device cross section divided by the number of cells in the device.

The upper bound given by (5) was actually derived for an individual cell rather than an entire device. The bound can be applied to devices by summing over cells. If we apply (5) to each cell and sum over cells, we obtain the same result (5), except that the cross sections are now sums of cell cross sections. *These sums are U-type device cross sections. Therefore, for devices susceptible to MBU, the σ_{hi} to be used in (5) is the U-type device cross section.*

DRAMs are especially prone to MBU, and they are also especially prone to cosine-law errors. The U-type device heavy-ion cross sections (and therefore the cell cross sections) for DRAMs are sometimes better described as isotropic than by the cosine law (the G-

type may have some other angular dependence, but this is not related in a simple way to the cell cross section). Therefore, data intended to represent the heavy-ion susceptibility of a DRAM at normal incidence should be measured at normal incidence, as opposed to using an assumed cosine-law conversion with data measured at angles.

VI. COMPARISONS WITH MEASURED DATA

Calvel *et al.* [8] and Petersen [9] each compiled a list of devices tested for SEU using both heavy-ions and protons. Weibull parameters for the heavy-ion cross sections were provided for each device, so an upper bound estimate for σ_{pr} is easily calculated from (10), using a computer code that calculates heavy-ion SEU rates and that accepts Weibull parameters as input. The calculated and measured saturation proton cross sections are compared in Table 2 (no distinction is made here between the saturation cross section and the cross section at E= 200 MeV). SEU data in the upper block in the table are from Calvel *et al.* [8]. Data from Petersen [9] that are not already in the upper block are in the second block (excluding two devices as discussed at the end of this section). The Weibull parameters are included in the table so that readers possessing a computer code as discussed above can easily reproduce the estimates for σ_{pr}. SEL data for the last two devices (lower block) in the table were discussed in previous sections. The last column is the calculated σ_{pr} divided by the measured σ_{pr}.

Note that the upper bound is within a factor of three of the measured cross section for most of the SEU cases listed. The SEL entries are consistent with a known trend. Given two devices having the same σ_{hi} curve, but one refers to SEU and the other refers to SEL, the proton cross section is usually (perhaps not always) smaller for the SEL case. Therefore the upper bound estimate will often be excessively conservative for SEL (e.g., the HM65162). However, the K-5 shows that there are also cases in which the upper bound is only moderately conservative.

Two devices were omitted from the second block in Table 2. One is the AMD version of the 93L422. The upper bound estimate for this device under-estimated the reported

proton cross section by a factor of six, and this motivated a search for the original data. This search revealed that the Weibull fit in [9] under-estimates the heavy-ion cross section data [10] by a consistent (various LET) factor of either about two or three, depending on which of the two tested devices is selected for comparison. It was also found that scatter in the proton data [11] spans a factor of five, with the most pessimistic data point used in the subsequent literature (internal JPL memos commented on large part-to-part variations, and problems with proton-beam control and dosimetry). While these data are adequate for SEU rate estimates, the precision is inadequate for testing or refining theoretical models. Incidentally, this search also revealed considerable part-to-part variations in the Fairchild version of the 93L422 (internal JPL memos), so the slight under-estimation in Table 2 for this device is not too alarming. The other omitted device is the 2164. The upper bound estimate for this device under-estimated the reported proton cross section by a factor of almost two, and this motivated another search for the original data. It was found that several types of heavy-ion cross sections were measured [12], but the type used in the subsequent literature is the G-type discussed in Section V.D. The U-type required for proton cross section estimates is about twice the G-type.

Part	Weibull Parameters (L_0 and W in MeV-cm^2/mg, C in cm^2)				Data	Upper Bound	Ratio
	L_0	C	W	S	σ_{pr}(sat.) (cm^2)	σ_{pr}(sat.) (cm^2)	
SMJ44100 (SEU)	1.39	2.0E0	15.0	1.21	7.00E-7	1.9E-6	2.7
62256R (SEU)	1.60	6.4E-1	20.0	1.65	1.47E-7	3.8E-7	2.6
IBM 16MEG (SEU)	1.70	1.3E-1	20.0	3.00	2.12E-8	5.8E-8	2.7
MT4C1004C (SEU)	1.54	1.3E0	14.5	1.45	3.94E-7	1.0E-6	2.5
KM41C4000Z-8 (SEU)	1.52	1.3E0	18.0	1.45	3.27E-7	8.9E-7	2.7
01G9274 (SEU)	1.60	9.7E-2	28.0	3.25	4.19E-9	3.1E-8	7.4
OW 62256 (SEU)	2.40	4.3E-1	16.5	2.25	8.70E-8	2.3E-7	2.6
MT4C4001 (SEU)	1.49	1.3E0	15.0	1.21	2.94E-7	1.2E-6	4.1
HM6116 (SEU)	4.20	6.6E-2	7.9	2.50	4.59E-8	4.7E-8	1.0
62832H (SEU)	3.40	1.0E-1	20.0	1.50	2.89E-8	5.0E-8	1.7
2901B (SEU)	4.20	3.0E-3	10.0	1.50	8.5E-10	2.1E-9	2.5
TC514100Z-10 (SEU)	0.86	2.1E0	18.0	1.15	1.00E-6	2.0E-6	2.0
HM 65656 (SEU)	1.50	1.1E-1	12.0	1.75	2.98E-8	9.6E-8	3.2
MB814100 10PSZ (SEU)	1.15	3.2E0	15.0	1.35	6.90E-7	2.9E-6	4.2
HYB514100J-10 (SEU)	0.86	2.1E0	14.0	1.10	1.46E-6	2.5E-6	1.7
LUNA C (SEU)	3.20	1.5E-1	14.0	3.00	2.12E-8	8.2E-8	3.9
D424100V-80 (SEU)	0.80	1.5E0	10.0	1.10	1.76E-6	2.3E-6	1.3
HM6516 (SEU)	5.00	3.0E-2	14.0	1.90	2.46E-9	1.6E-8	6.5
Fairchild 93L422 (bipolar) (SEU per bit)	0.6	2.6E-5	4.4	0.7	1.4E-10	9.6E-11	0.70
Samsung 16M 3.3V DRAM (SEU per bit)	0.6	9.87E-8	16.39	1.85	3.5E-14	7.4E-14	2.1
Hitachi 16M 3.3V DRAM (SEU per bit)	0.5	2.27E-8	7.9	4.11	1.6E-14	2.4E-14	1.5
Micron 16M 3.3V DRAM (SEU per bit)	0	1.92E-8	8.98	5.37	8.0E-15	1.9E-14	2.3
IBM E 16M 3.3V DRAM (SEU per bit)	-0.4	2.6E-9	7.89	5.39	1.7E-15	2.8E-15	1.6
K-5 (SEL)	NA: See Section V.C				5.6E-9	1.9E-8	3.4
HM65162 (1985) (SEL)	NA: See Section V.A				1.4E-10	2.9E-8	210

Table 2: Comparison between predicted and measured proton saturation cross sections. Data in the first block are from Calvel *et al.* [8], and data in the second block are from Petersen [9]. Devices in the third block were discussed in earlier sections.

VII. EQUALITIES FOR SEVERAL SPECIAL CASES

This section derives equalities (instead of inequalities or bounds) for several special cases. The results have limited practical applications because they are only useful for SEU or SEL rate calculations if we have information that is rarely available. Future work may find ways to obtain the required information, but another motivation for this section is academic curiosity. It is interesting to see the similarities and differences between various cases. Furthermore, the results derived in this section can be compared to results previously derived by other investigators. This comparison is made in the next section.

A. Case 1: A Single but Arbitrary SV

The first special case is a single SV having an arbitrary shape. The thickness measured in the vertical direction can vary with the lateral coordinates. This variable thickness accounts for the gradual increase in the normal-incident $\sigma_{hi}(L)$ versus L curve. Using Ω=1 inside the SV and Ω=0 outside, (2) and (3) reduce to

$$\sigma_{pr}(E) = n\,\alpha(E,Q_c)\int_{SV} d^3x\,, \quad \int_0^\infty \frac{1}{L}\frac{d\sigma_{hi}(L)}{dL}\,dL = \frac{a}{Q_c}\int_{SV} d^3x$$

which gives

$$\sigma_{pr}(E) = \frac{Q_c\, n\,\alpha(E,Q_c)}{a}\int_0^\infty \frac{1}{L}\frac{d\sigma_{hi}(L)}{dL}\,dL\,. \tag{12}$$

Note that if it is somehow known that the single SV model does apply to a device, but Q_c is unknown, then the supplementary information (that the single SV model applies) cannot be used to reduce the bound given by (5). Without knowing Q_c, the best bound obtainable for (12) is still given by (5). In fact, we see from (12) that the upper bound given by (5) is not overkill, because this limit can be reached by any device adequately described by the single SV model and having a special value for the critical charge. This special value is the maximizing Q in (4). Using the data in Table 1, we calculate this maximizing Q (which is 1/B) to be about 0.1 pC when E=200 MeV.

The assumption that Ω=1 inside the SV is appropriate when Q_c is the critical value of the charge liberated within the SV. If the SV is subject to some kind of transistor gain amplification, the charge collected at a device contact could differ from the liberated charge. For example, if an amplification results in the collected charge being twice the liberated charge, and if Q_c refers to the critical value of the collected (or amplified) charge instead of the critical value of the liberated charge, then Ω=2 inside the SV. A generalization of (12), which allows Ω to be any positive constant (denoted Ω_0) in the SV is

$$\sigma_{pr}(E) = \frac{1}{a}\frac{Q_c}{\Omega_0} n\,\alpha(E, \frac{Q_c}{\Omega_0}) \int_0^\infty \frac{1}{L}\frac{d\sigma_{hi}(L)}{dL} dL .$$

B. Case 2: A Collection of RPPs having a Distribution of Critical Charges

Previous results apply to a device having a single value of Q_c. A device containing several components, having different values of Q_c, can be treated by simply adding the cross sections for each component. The postulate behind the IRPP method for calculating heavy-ion rates [6] is that there is a collection of RPP shaped SVs producing a distribution of values of Q_c. The gradual increase in the heavy-ion cross section with increasing ion LET is attributed to an increasing number of contributing RPPs with increasing LET. To describe this case, we can use (12) for each RPP (the heavy-ion cross section in (12) becomes a step function when applied to an RPP, allowing the right side to be expressed without an integral), and sum (or integrate) the individual RPP cross sections to obtain the device cross section. The result need not be listed here because it is identical to the result derived in Case 4 discussed later. The two cases produce the same result because of a mathematical equivalence pointed out in the discussion of Case 4.

C. Case 3: A Partially Separable Ω

This case applies when Ω can be adequately approximated by a partially separable function; a function of z alone times a function of x and y alone (z measures depth, and x and y are two lateral coordinates). We write Ω as

$$\Omega(x, y, z) = f(x, y)\, g(z) \tag{13}$$

for some functions f and g. This equation can be written as

$$\Omega(x, y, z) = \tau(x, y)\frac{g(z)}{I} \tag{14}$$

where the charge-collection depth τ and the integral I are defined by

$$\tau(x, y) \equiv \int_{-\infty}^{\infty} \Omega(x, y, z)\, dz = f(x, y)\, I\,, \quad I \equiv \int_{-\infty}^{\infty} g(z)\, dz\,.$$

Substituting (14) into (2) gives

$$\sigma_{pr}(E) = \int G(E, \tau(x, y))\, dxdy$$

where G is defined by

$$G(E, \xi) \equiv n\int_{-\infty}^{\infty} \alpha(E, \frac{Q_c\, I}{\xi\, g(z)})\, dz\,. \tag{15}$$

It is shown in the appendix that the above equation for σ_{pr} can be written as

$$\sigma_{pr}(E) = \int_0^{\infty} G(E, \frac{Q_c}{a\, L})\frac{d\sigma_{hi}(L)}{dL}\, dL\,. \tag{16}$$

D. Case 4: Lateral Variation within a Uniform Contributing Depth

This case, which is a further specialization of the previous case, assumes that charge collection is confined to a horizontal layer having a uniform thickness T. Ω is independent of z (but it may still depend on the lateral coordinates) within this layer, and Ω=0 above or below this layer. This case is obtained from Case 3 by letting g in (13) satisfy I/g(z)=T when z is inside the horizontal layer, and g(z)=0 when z is outside. For this case, (15) reduces to

$$G(E,\xi) = n\,\alpha(E, \frac{Q_c\,T}{\xi})\,T$$

and (16) becomes

$$\sigma_{pr}(E) = T\int_0^\infty n\,\alpha(E, aLT)\frac{d\sigma_{hi}(L)}{dL}\,dL. \qquad (17)$$

This result also applies to the collection of RPPs (Case 2) with T the RPP thickness, because there is a mathematical equivalence between that case and the present case. The equivalence applies to normal-incident heavy ions (note that unlike the integral in (5) and (12), the integral in (17) is not rotationally invariant, so the heavy-ion data must refer to normal incidence). The equivalence is due to the fact that (for normal-incident hits) an Ω that varies with the lateral coordinates combined with a constant Q_c (this case) is equivalent to a Q_c that varies with the lateral coordinates (from one RPP to the next) combined with a constant Ω (Case 2).

It is interesting that (17) is not equivalent to the result (12) for a single but general SV (Case 1). A comparison between the two equations shows a fundamental difference between a collection of RPPs and a single but general SV (having a variable thickness), even though both cases can produce the same σ_{hi} curve. The same σ_{hi} curve can lead to different estimates for σ_{pr}, depending on which model is assumed to apply. A device described by both Case 1 and Case 4 (or Case 2) is characterized by an SV with uniform depth, so the heavy-ion cross section curve is a step function and the two equations, (12) and (17), give the same result. Otherwise, the two equations give different results, and (17) can be used to obtain a smaller (better) upper bound for σ_{pr} than given by (5), *if it is somehow known that Case 4 (or Case 2) really does apply*, but T is unknown. This bound is obtained by selecting T to maximize the right side of (17). That this bound is better (or the same, for very special cases) than given by (5) can be seen by noting that the upper bound of a sum is less than or equal to the sum of upper bounds. In this context, the sum (or integral) of upper bounds has the maximizing operation moved inside the integral in (17), so the maximizing T is selected independently for each value of L. This sum of

upper bounds is the right side of (5), while the upper bound of the sum is the improved upper bound obtained from (17). Therefore, *if it is somehow known that Case 4 (or Case 2) really does apply*, but T is unknown, then the supplementary information (that Cases 2 or 4 apply) *can* be used to reduce the bound given by (5).

VIII. SOME RECENT WORK

A number of results relating proton cross sections to heavy-ion cross sections have been presented in the recent literature. One motivation for discussing some of these results here is to acknowledge some of the recent work previously done by others. In particular, the result for Case 2 (Section VII) was previously derived by Normand, as discussed below. Another motivation for discussing these results is that it is interesting to see the similarities and differences between various theories. These similarities and differences become clear after recognizing that various results are special cases of (and easily reproduced from) the more general theory in the present paper. In particular, it will be seen that a result by Normand and a result by Johnston *et al.* were derived from physically different but mathematically equivalent assumptions (Case 2 versus Case 4 in Section VII), except that Johnston used an approximation for $n\alpha$. The risk associated with using measured proton cross sections to estimate heavy-ion rates, as suggested by O'Neill *et al.*, is also discussed.

A. Normand's Result

An equation resembling (17) was previously derived by Normand (equation (6) in [2]) from the physical assumptions under Case 2 in Section VII [13]. Apart from notation, the equations differ in that Normand's equation contains an additional parameter C, which was first introduced in an earlier paper [14]. Comparisons between model predictions and measured proton cross sections indicated that C=0.5 is appropriate for some cases, while C=1 is appropriate for some other cases [2]. This parameter C is supported by physical arguments, and these arguments can be used to modify (17) as shown below.

The derivation of (17) started with one Ω function applicable to all ionization sources, but a different Ω for different sources may actually be appropriate, depending on whether the ionization produces high-density conditions (the carrier density liberated by the ionization greatly exceeds the doping density) or low-density conditions. For the high-density case, a low-order approximation for collected current at a reversed-biased depletion region boundary (DRB) is twice the minority carrier diffusion current, with the carrier-density gradient (used to calculate the diffusion current) calculated from the ambipolar diffusion equation [15]. However, for low-density conditions at the DRB, the current is the minority carrier diffusion current instead of twice this current. Assuming that the high-density case applies to heavy ions, while proton reaction products create conditions ranging anywhere between low-density and high-density, the Ω appropriate for proton reactions is somewhere between 0.5 and 1 times the Ω appropriate for heavy ions. If Ω refers to heavy ions, then (2) should be modified by replacing Ω with CΩ, where C is some number between 0.5 and 1. Repeating the derivation of (17) while using the modified form of (2) gives

$$\sigma_{pr}(E) = T \int_0^\infty n\,\alpha(E, aL\frac{T}{C})\frac{d\sigma_{hi}(L)}{dL}\,dL .$$

As long as T is regarded as a fitting parameter, and not given a literal interpretation, the equation is just as convenient when expressed in terms of another fitting parameter T'≡T/C. In terms of T', the equation becomes

$$\sigma_{pr}(E) = C\,T' \int_0^\infty n\,\alpha(E, aLT')\frac{d\sigma_{hi}(L)}{dL}\,dL$$

which conforms to Normand's result.

B. Barak's Result

A result presented by Barak *et al.* (equation (6) in [16]) has the same form as (17). The two equations can be given a more similar appearance by changing variables from L to ε in (17), using ε=LT, and then integrating (17) by parts. However, a distinguishing characteristic of their work is that nα in (17) is replaced by an experimentally measured

function (describing the spectra of charge liberated in surface barrier detectors via proton reactions) which is not subject to errors associated with the second physical postulate in Section II. Unfortunately, this replacement for $n\alpha$ appears to be justified only for the conditions assumed under Case 2. Perhaps their work will inspire future work that will improve upon the second physical postulate while still retaining most of the generality allowed by the first physical postulate.

C. Johnston's Result

An analysis by Johnston *et al.* [17] recognized that the collected charge relevant to heavy-ion induced SEL is a function of the lateral coordinates of the ion-hit location. This is consistent with Case 4, and an equation used by Johnston for calculating proton SEL cross sections can be reproduced by applying an approximation to (17). This approximation, which was used by Johnston, replaces a distributed spectrum of proton-induced reaction products with one predominant or representative type of reaction, in which the deposited energy is about 10 MeV (the liberated charge is about 0.46 pC, which is the number used by Johnston). The entire (i.e., includes all high-energy interactions) proton cross section is associated with this reaction, so $n\alpha$ is approximated by a step function given by

$$n\,\alpha(Q) = 2.5\times10^{-6}\,/\,\mu m \;\; if \;\; Q \le 0.46\;pC, \qquad n\,\alpha(Q) = 0 \;\; if \;\; Q > 0.46\;pC.$$

Substituting this step function for $n\alpha$ into (17) gives

$$\sigma_{pr} = \frac{T}{4\times10^{5}\,\mu m}\,\sigma_{hi}\left(\frac{44\mu m}{T}\,\frac{MeV\,cm^{2}}{mg}\right). \tag{18}$$

When $n\alpha$ is a distributed spectrum, the heavy-ion cross section over a range of LET values contributes to σ_{pr}. The fact that σ_{hi} is evaluated at only a single point in (18) is an artifact of the step-function fit used for $n\alpha$. The selected step function might be the best of the step-function fits for the intended application, because Johnston *et al.* [17] found good agreement between the measured and predicted σ_{pr} for a number of cases

representing a wide range of technologies. However, it is not yet clear whether this approach has limitations.

A distinguishing characteristic of their work is in the selection of a value for T. T was taken to be the epi-layer thickness for the epitaxial devices, but the bulk devices require more thought. Computer simulations have shown that Case 4 does not apply to the bulk devices (of the cases considered in Section VII, Case 3 is the only possible candidate). Therefore, T does not have a literal interpretation as assumed in Case 4, and some effective value is needed. From the point of view of Case 4, T is a constant and is not necessarily the same as the charge-collection depth (which is a function of the lateral coordinates). The value that Johnston assigned to T was the charge-collection depth calculated by computer simulations at the lateral center of a cylindrically symmetric device (the charge-collection depth is expected to be maximum at the lateral center). Johnston *et al.* provided a recipe instead of an equation, but the numerical entries in their Table 2 (in [17]) can be reproduced by using (18) with T obtained from their Figure 5 (in [17]).

D. O'Neill's 1997 Results

A sophisticated technique by O'Neill *et al.* [18] calculates a spectrum of proton-induced liberated charge, which is a replacement for $n\alpha(Q)$ in (17) that is not subject to errors associated with the second physical postulate in Section II. The end result of this work is a statement regarding heavy-ion induced SEU rates derived from measured proton cross sections. The authors' intention is only to show a trend, and they warn the reader not to rely too heavily on proton data for heavy-ion rates, so a high level of rigor is not required in their work. Unfortunately, in spite of this warning, some individuals *are* relying on proton data in lieu of heavy-ion data [19]. It is therefore important to point out that while the level of rigor in O'Neill's work is adequate for the intended purpose (to establish a trend), there are still some weak points in the analysis that make it unsuitable for applications requiring a very high confidence level.

One weak point of the analysis is that charge collection is assumed to be as described by the SV model, where the SV is a thin RPP (the thickness is ~1 μm, with lateral dimensions much larger than the thickness). This assumption has severe limitations, but for those cases in which it does apply, the authors provide the appropriate replacement, for $n\alpha(Q)$, which is the spectrum of charge liberated in this RPP via proton reactions. An effective LET associated with a proton reaction is calculated by dividing the liberated charge by the RPP thickness. Effective LET and liberated charge are equivalent descriptions, because one is proportional to the other. However, the second weak point is that the proton-induced spectrum, plotted as a function of effective LET, is compared to a heavy-ion spectrum representing a space environment but plotted as a function of ion LET rather than effective LET. This comparison would be meaningful if all heavy-ions in space hit the RPP at normal incidence, but they don't. For hits at angles, there is also an effective LET for heavy-ions (also defined in terms of liberated charge divided by RPP thickness). Heavy-ion hits that liberate a charge exceeding the maximum that is possible from proton reactions are predicted to be infrequent if we assume (as the authors did) that such events require high-LET ions (which have a low abundance). However, such events are seen to be much more frequent if we recognize that they can also be caused by low-LET (and very abundant) ions hitting the RPP at angles.

The second weak point can be removed by slightly modifying the arguments used by the authors. The basic idea is to compare the proton-induced spectrum to an *effective flux* describing heavy ions. An effective flux is a characteristic of both the environment and an assumed directional dependence describing device susceptibility to heavy ions. An effective flux for a given heavy-ion environment is different for devices having a nearly isotropic heavy-ion cross section than for devices described by the cosine law (e.g., an RPP with thickness much smaller than the lateral dimensions). Effective flux can be rigorously defined if we can find a function K satisfying

$$\sigma(L,\theta,\phi) = \int_0^\infty K(L', L, \theta, \phi) \frac{\partial \sigma_N(L')}{\partial L'} dL' \tag{19}$$

where $\sigma(L,\theta,\varphi)$ is the directional heavy-ion cross section evaluated at ion LET L and in the direction described by the spherical-coordinate angles θ (measured from the device normal) and φ, and σ_N is the normal-incident heavy-ion cross section. The σ_N here is the same as σ_{hi} in (17), but the symbolism was changed to distinguish normal incidence from other directions. The function K has a simple interpretation for devices described by Case 2 and with geometrically similar RPPs (i.e., each ratio of dimensions for one RPP equals the corresponding ratio for all other RPPs). For this case, $K(L',L,\theta,\varphi)$ can be shown to be the normalized (by dividing by the area of the RPP face seen at normal incidence) directional cross section for an RPP having normal-incident threshold LET L'. $K(L',L,\theta,\varphi)$ does not depend on the size of the RPP, but it does implicitly depend on the RPP dimension ratios, and explicitly depends on the threshold LET L' of the RPP. The heavy-ion SEU rate r_{hi} can be calculated from

$$r_{hi} = \int_0^{\infty} \int_{-1}^{1} \int_0^{2\pi} h(L,\theta,\phi)\, \sigma(L,\theta,\phi)\, d\phi\, d(\cos\theta)\, dL$$

where h is the differential (in LET) directional flux. Substituting (19) into the above equation gives

$$r_{hi} = \int_0^{\infty} H_{eff}(L') \frac{\partial}{\partial L'} \sigma_N(L')\, dL' \tag{20}$$

where H_{eff} is the integral effective flux defined by

$$H_{eff}(L') \equiv \int_0^{\infty} \int_{-1}^{1} \int_0^{2\pi} h(L,\theta,\phi)\, K(L',L,\theta,\phi)\, d\phi\, d(\cos\theta)\, dL\,. \tag{21}$$

From the interpretation of K as a normalized directional cross section for an RPP, it is seen from (21) that H_{eff} is the normalized SEU rate for the RPP. This makes effective flux associated with Case 2 very easy to calculate via a standard computer code that calculates heavy-ion SEU rates for RPPs. We calculate the SEU rate for the RPP, divide by the area of the face seen at normal incidence, and plot this normalized rate as a function of the threshold LET assigned to the RPP. The calculated effective flux will be independent of the thickness assigned to the RPP, as long as corresponding values are assigned to the

critical charge (to be consistent with the selected threshold LET) and to the lateral dimensions (to be consistent with the selected dimension ratios).

To be consistent with O'Neill *et al.* [18], we now assume Case 2 conditions with all RPPs having the same thickness T, so (17) applies. The $n\alpha(Q)$ is taken to be the spectrum calculated by the authors so that errors associated with the second physical postulate are removed. We next look for a constant A satisfying

$$A\,T\,n\,\alpha(a\,L\,T) \geq H_{eff}(L) \quad for\ all\ L \tag{22}$$

if it exists. If such an A can be found, we can use (22) with (17) and (20) to obtain an upper bound on the heavy-ion rate given by

$$r_{hi} \leq A\,\sigma_{pr}\,. \tag{23}$$

The result (23), which is an extension of the authors' earlier work, accounts for directional effects, but there are still some serious limitations. The first is that an RPP with a known thickness T is assumed to apply. This might adequately describe some cases, but the assumption is unreliable. Even for those cases in which the assumption is adequate, there is still a second limitation in that an A satisfying (22) may not exist. Such an A can be found for some cases. In particular, the galactic cosmic ray heavy-ion environment for a low-altitude, low-inclination Earth orbit is limited to very low-LET (very high-energy) particles, so the raw flux H does not extend to high LET. Furthermore, the effective flux H_{eff} appropriate for devices having a nearly isotropic heavy-ion cross section is nearly the same as the raw flux H, so H_{eff} does not extend to high LET for this case. In contrast, H_{eff} for cosine-law devices extends to much higher LET than H. Therefore, an A satisfying (22) might be found for isotropic devices in such an orbit, but not for cosine-law devices (note that H_{eff} implicitly depends on the ratio of T to the lateral RPP dimensions, with a small ratio producing the cosine law). An approach that might be used when there is no A satisfying (22) is to express the effective flux as a sum of two components constructed so that there is an A associated with one of the components. It is necessary to find separate arguments applicable to the other flux component (e.g., its contribution to the heavy-ion rate is smaller than some number

because this flux is small). Bounds such as (23) probably have some applications, and might correctly predict some trends, but the first limitation discussed above makes them unreliable.

E. O'Neill's 1998 Results

Another analysis by O'Neill *et al.* [20] also leads to a conclusion regarding heavy-ion induced SEU or SEL rates derived from measured proton cross sections. Again, a comparison is made between a proton-induced spectrum and a heavy-ion spectrum. This analysis does not repeat the error discussed in the previous subsection, because all spectra now refer to particle LET instead of effective LET, so comparisons are between similar types of spectra. However, the effect of limited particle range on collected charge limits the applicability of this work. Proton-induced reaction products having ranges less than 5 μm were assigned a reduced LET to compensate for range effects, but no other distinction was made between the reaction products and long-range particles (cosmic rays) having the same LET. This limits the cases that can be treated by this analysis, because charge-collection depths can be quite long (sometimes 20 μm for SEL [17]). Furthermore, in order for the charge-collection depth to be useful for describing collected charge, the ion range must be considerably longer than this depth, even for hypothetical ion tracks (which can be treated by computer simulations) having a constant LET over the ion range [17]. This is because the contributing depth is greater than the charge-collection depth, as noted in Section IIB. The most unfortunate property of the SV model is that it does not sufficiently emphasize the importance of ion range. In fact, even some of the heavy ions used for tests at accelerators sometimes underestimate SEL cross sections because of inadequate range.

The authors' intention is only to show a trend, and they warn the reader not to rely too heavily on proton data for heavy-ion rates, so the assumptions are adequate for the intended purpose. In fact, this work has an impressive track record, in the sense that predictions agreed with observations for many cases. However, in view of the discussion in the previous paragraph, some exceptions can be anticipated. An example is SEL in the

HM65162 manufactured in 1986. No events were observed from a proton fluence of 10^{11}/cm^2 [5], but the heavy-ion threshold LET was about 2.5 MeV-cm^2/mg, with a saturation cross section exceeding 2×10^{-2} cm^2 (from Fig.1 in [5]). This device is extremely susceptible to SEL from heavy ions, but the proton data give no warning of this. It is clear from this example that proton data are inadequate for devices exposed to heavy ions when a very high confidence level is required.

F. The Petersen-Barak Equation

Barak *et al.* [3] pointed out that empirical fits provided by Petersen [9] can be combined to give

$$\sigma_{pr} = 2.22\times10^{-5}\,\frac{\sigma_{hi,0}}{(L_{0.25}{}^{\#})^2} \tag{24}$$

where $\sigma_{hi,0}$ is the heavy-ion saturation cross section, σ_{pr} (throughout this section) is the saturation cross section for protons, and $L_{0.25}$# is the numerical part (when the units are MeV-cm^2/mg) of $L_{0.25}$ defined by $\sigma_{hi}(L_{0.25})=0.25\times\sigma_{hi,0}$. When Weibull parameters are given, $L_{0.25}$ can be calculated from

$$L_{0.25} = L_0 + (0.288)^{1/S}\times W .$$

This paper calls (24) the Petersen-Barak equation. This equation can be reproduced (approximately) by assuming that Case 1 applies and using (6) to write (12) as

$$\sigma_{pr} = \frac{Q_c}{a} A\, e^{-B Q_c} \int_0^{\infty} \frac{1}{L}\frac{d\sigma_{hi}(L)}{dL}\, dL \tag{25}$$

where the E dependence was omitted from the notation because 200 MeV is assumed. Let $\tau_{0.25}$ be the charge-collection depth at the perimeter of the region represented by the cross section $\sigma_{hi}(L_{0.25})$. The critical LET for ion hits at this perimeter is $L_{0.25}$, so

$$Q_c = a\,\tau_{0.25}\,L_{0.25}$$

and (25) becomes

$$\sigma_{pr} = \tau_{0.25}\, L_{0.25}\, A\, e^{-a\, B\, \tau_{0.25}\, L_{0.25}} \int_0^{\infty} \frac{1}{L} \frac{d\sigma_{hi}(L)}{dL}\, dL. \tag{26}$$

To obtain the desired result, we use the ad hoc assumption

$$\tau_{0.25} = 3.38\ \mu m. \tag{27}$$

Using (27) and Table 1 with (26) gives

$$\sigma_{pr} = 6.76\times10^{-6}\, L_{0.25}\, e^{-0.349\, L_{0.25}} \int_0^{\infty} \frac{1}{L} \frac{d\sigma_{hi}(L)}{dL}\, dL. \tag{28}$$

When the σ_{hi} curve is defined by a Weibull fit (as opposed to alternatives such as (7)), a fairly good approximation is

$$\int_0^{\infty} \frac{1}{L} \frac{d\sigma_{hi}(L)}{dL} dL \approx \frac{\sigma_{hi,0}}{L_{0.25}}. \tag{29}$$

Another approximation is

$$e^{-X} \approx \frac{0.4}{X^2} \quad (\textit{within a factor of } 1.4 \textit{ when } 0.8 \le X \le 4.0). \tag{30}$$

The relevant values of X in (30) depend on $L_{0.25}$. For many (not all) devices in Table 2, the relevant X results in (30) being accurate to within a factor of 1.4 (either too small or too large). Applying the approximations (29) and (30) to (28) produces the Petersen-Barak equation (24).

Because approximations were used to derive (24) from (28), we might expect (24) to be less accurate than (28). It turns out that (24) has a better track record than (28). The device data in Table 2 (excluding the SEL cases) were used to construct Table 3. The ratio columns give σ_{pr} calculated from the indicated equation divided by the measured σ_{pr}. Note that the ratio from (24) is usually closer to 1 than the ratio from (28). Other values for $\tau_{0.25}$ were tried with (28), but did not improve the track record for (28) when a common value for $\tau_{0.25}$ is assigned to all devices.

Part	Ratio from (24)	Ratio from (28)
SMJ44100	1.39	1.60
62256R	0.796	0.578
IBM 16MEG	0.613	0.213
MT4C1004C	1.24	1.31
KM41C4000Z-8	1.06	0.969
01G9274	1.20	0.106
OW 62256	0.776	0.469
MT4C4001	2.09	2.40
HM6116	0.394	0.375
62832H	0.522	0.293
2901B	1.07	0.999
TC514100Z-10	0.963	1.16
HM 65656	1.50	1.72
MB814100 10PSZ	2.03	2.36
HYB514100J-10	1.10	1.35
LUNA C	1.01	0.599
D424100V-80	1.17	1.22
HM6516	1.80	1.01
Fairchild 93L422 (bipolar)	2.26	0.542
Samsung 16M 3.3V DRAM	0.779	0.789
Hitachi 16M 3.3V DRAM	0.785	0.976
Micron 16M 3.3V DRAM	1.05	1.30
IBM E 16M 3.3V DRAM	0.971	1.17

Table 3: The ratio columns give σ_{pr} calculated from the indicated equation (using data in Table 2) divided by the measured σ_{pr}. Note that the Petersen-Barak equation (24) performs better (the ratio is closer to 1) than (28) for most of the cases listed.

A suggested explanation as to why (24) fits the data better than (28) is that (28) assigns the same $\tau_{0.25}$ to all devices. Perhaps some other parameter is better than $\tau_{0.25}$ in the sense of being approximately the same for many devices. We could consider a common value for Q_c, instead of $\tau_{0.25}$, for all devices. A common Q_c produces estimates that are a common multiple of the upper bounds in Table 2. Selecting Q_c to make the estimates equal to one-half the upper bounds will produce a moderately good track record, but still not as good as (24).

Assigning a common $\tau_{0.25}$ to all devices does not (at least not when Case 1 is assumed) fit the statistical trend as well as (24), and assigning a common Q_c to all devices does not fit the statistical trend as well as (24). That (24) performs better than the above alternatives is not an accident, because (24) originated from empirical fits to extensive data sets. The property of being an empirical fit gives (24) an advantage and a disadvantage compared to a physics-based model. The disadvantage is that information sufficient to completely determine σ_{pr} cannot be utilized by (24), even if such information were available. The advantage is that, when such information is not available (usually the case in practice), (24) has a high probability of producing an estimate that is nearly as good or better than a physics-based model containing ad hoc values for the unknown parameters.

IX. CONCLUSIONS

A common situation is that in which a device has been tested with heavy ions for SEU and/or SEL, but not yet tested with protons. A proton test is an additional expense, so there is a motivation to use heavy-ion data to predict proton cross sections. Of the results derived here, the upper bound estimate is the most useful in terms of practical applications, because it is derived from the most generic assumptions and does not require information that is not available. A disadvantage is that this estimate is sometimes excessively conservative (pessimistic). The method was used to estimate SEU rates in a proton environment for numerous devices of interest to a JPL flight project. An additional (but not excessive) conservatism was included by assigning the 200 MeV cross section to

all protons having energies greater than 7 MeV. The observation from this application is that the rate estimates are often acceptable to a flight project, even though the estimates might be excessively conservative, in which case a proton test is not needed. If the estimate predicts problems for a flight project, a proton test is needed to obtain a smaller estimate, but the upper bound does at least reduce the number of tests that are required.

Practical applications of the results intended to accurately estimate the proton cross section (instead of a bound for it) are more limited, because additional information is required. It must first be known which model (e.g., one of the cases in Section VII) is the best choice, and then model parameters must be estimated. If it is (somehow) known that Case 1 is an adequate approximation, an estimate is needed for the critical charge. If it is (somehow) known that either Case 2 or Case 4 is an adequate approximation, an estimate is needed for the RPP thickness or the contributing depth. If it is (somehow) known that the latter cases are inappropriate, but the more versatile Case 3 is an adequate approximation, an estimate is needed for the function g(z). Future work might find inexpensive methods for obtaining the required information, but another reason for presenting these results is academic curiosity. It is interesting to see the similarities and differences between various models, including models previously presented by others.

An empirical fit applicable to SEU (not SEL), which this paper calls the Petersen-Barak equation, was also discussed. This is not only one of the simplest results, but also has a high probability of producing an estimate for the saturation proton cross section that is nearly as good or better than a physics-based model containing ad hoc values for unknown parameters. If the information that is needed to take full advantage of a physics-based model is not available (usually the case), and if the objective is to obtain a "most probable estimate", as opposed to an upper bound, this equation should be considered.

Previous work regarding heavy-ion rate estimates, or bounds, derived from measured proton data was discussed. Although this work successfully predicted trends, it is suggested here that proton data are inadequate for such applications when a high confidence level is required.

REFERENCES

[1] J. Barak, J. Levinson, A. Akkerman, E. Adler, A. Zentner, D. David, Y. Lifshitz, M. Hass, B.E. Fischer, M. Schlogl, M. Victoria, and W. Hajdas, "Scaling of SEU Mapping and Cross Section, and Proton Induced SEU at Reduced Supply Voltage," *IEEE Trans. Nucl. Sci.*, vol. 46, no. 6, pp. 1342-1353, Dec. 1999.

[2] E. Normand, "Extensions of the Burst Generation Rate Method for Wider Application to Proton/Neutron-Induced Single Event Effects," *IEEE Trans. Nucl. Sci.*, vol. 45, no. 6, pp. 2904-2914, Dec. 1998.

[3] J. Barak, R.A. Reed, and K.A. LaBel, "On the Figure of Merit Model for SEU Rate Calculations," *IEEE Trans. Nucl. Sci.*, vol. 46, no. 6, pp. 1504-1510, Dec. 1999.

[4] L. Edmonds, "SEU Cross Sections Derived from a Diffusion Analysis," *IEEE Trans. Nucl. Sci.*, vol. 43, no. 6, pp. 3207-3217, Dec. 1996.

[5] J. Levinson, A. Akkerman, M. Victoria, M. Hass, D. Ilberg, M. Alurralde, R. Henneck, and Y. Lifshitz, "New Insight into Proton-Induced Latchup: Experiment and Modeling," *Appl. Phys. Lett.*, vol. 63, no. 21, pp. 2952-2954, Nov. 1993.

[6] E.L. Petersen, J.C. Pickel, J.H. Adams, Jr., and E.C. Smith, "Rate Prediction for Single Event Effects -- a Critique," *IEEE Trans. Nucl. Sci.*, vol. 39, no. 6, pp. 1577-1599, Dec. 1992.

[7] E.L. Petersen, "The Relationship of Proton and Heavy Ion Upset Thresholds," *IEEE Trans. Nucl. Sci.*, vol. 39, no. 6, pp. 1600-1604, Dec. 1992.

[8] P. Calvel, C. Barillot, P. Lamothe, R. Ecoffet, S. Duzellier, and D. Falguere, "An Empirical Model for Predicting Proton Induced Upset," *IEEE Trans. Nucl. Sci.*, vol. 43, no. 6, pp. 2827-2832, Dec. 1996.

[9] E.L. Petersen, "The SEU Figure of Merit and Proton Upset Rate Calculations," *IEEE Trans. Nucl. Sci.*, vol. 45, no. 6, pp. 2550-2562, Dec. 1998.

[10] D.K. Nichols, M.A. Huebner, W.E. Price, L.S. Smith, and J.R. Coss, *Heavy Ion Induced Single Event Phenomena (SEP) Data for Semiconductor Devices from Engineering Testing*, Jet Propulsion Laboratory Publication 88-17, July 1988.

[11] D.K. Nichols, W.E. Price, and J.L. Andrews, "The Dependence of Single Event Upset on Proton Energy (15-590 MeV)," *IEEE Trans. Nucl. Sci.*, vol. 29, no. 6, pp. 2081-2084, Dec. 1982.

[12] J.M. Bisgrove, J.E. Lynch, P.J. McNulty, W.G. Abdel-Kader, V. Kletnieks, and W.A. Kolasinski, "Comparison of Soft Errors Induced by Heavy Ions and Protons," *IEEE Trans. Nucl. Sci.*, vol. 33, no. 6, pp. 1571-1576, Dec. 1986.

[13] E. Normand and T.J. Baker, "Altitude and Latitude Variations in Avionics SEU and Atmospheric Neutron Flux," *IEEE Trans. Nucl. Sci.*, vol. 40, no. 6, pp. 1484-1490, Dec. 1993.

[14] A. Taber and E. Normand, "Single Event Upset in Avionics," *IEEE Trans. Nucl. Sci.*, vol. 40, no. 2, pp. 120-126, April 1993.

[15] L. Edmonds, "Electric Currents Through Ion Tracks in Silicon Devices," *IEEE Trans. Nucl. Sci.*, vol. 45, no. 6, pp. 3153-3164, Dec. 1998.

[16] J. Barak, J. Levinson, A. Akkerman, Y. Lifshitz, and M. Victoria, "A Simple Model for Calculating Proton Induced SEU," *Proc. RADECS 95*, Arcachon, France, pp. 431-436, Sept. 18-22, 1995.

[17] A. Johnston, G. Swift, and L. Edmonds, "Latchup in Integrated Circuits from Energetic Protons," *IEEE Trans. Nucl. Sci.*, vol. 44, no. 6, pp. 2367-2377, Dec. 1997.

[18] P. O'Neill, G. Badhwar, and W. Culpepper, "Risk Assessment for Heavy Ions of Parts Tested with Protons," *IEEE Trans. Nucl. Sci.*, vol. 44, no. 6, pp. 2311-2314, Dec. 1997.

[19] Private communications.

[20] P. O'Neill, G. Badhwar, and W. Culpepper, "Internuclear Cascade-Evaporation Model for LET Spectra of 200 MeV Protons," *IEEE Trans. Nucl. Sci.*, vol. 45, no. 6, pp. 2467-2474, Dec. 1998.

APPENDIX: A MATHEMATICAL ANALYSIS

Let the coordinate system be oriented so that the z axis is parallel to the heavy-ion trajectory. The device orientation relative to this coordinate system is arbitrary. For a normal-incident orientation, σ_{hi} is the normal-incident heavy-ion cross section. Otherwise, σ_{hi} is a directional cross section. The location of an ion trajectory is given by two coordinates x and y. Let Q(x,y) be the collected charge produced by an ion with LET L and having a trajectory at x,y. Using the selected device orientation to define the charge-collection efficiency function $\Omega(x,y,z)$, we have

$$Q(x, y) = a\, L \int_{-\infty}^{\infty} \Omega(x, y, z)\, dz\,. \tag{A1}$$

Note that $\sigma_{hi}(L)$ is the area of the set of points (x,y) in the plane satisfying

$$Q(x, y) > Q_c\,.$$

This set of points is the same as the set satisfying

$$\tau(x, y) > \frac{Q_c}{a\, L}$$

where τ is the normalized collected charge (also called the charge-collection depth) defined by

$$\tau(x, y) \equiv \frac{Q(x, y)}{a\, L} = \int_{-\infty}^{\infty} \Omega(x, y, z)\, dz\,. \tag{A2}$$

Therefore

$$\sigma_{hi}(L) = F(\frac{Q_c}{a\, L}) \tag{A3}$$

where F is defined by

$$F(v) \equiv \textit{area of the set of points } (x, y) \textit{ satisfying } \tau(x, y) > v,$$

i.e., F(v) is the cross section for the normalized charge to exceed v.

A mathematical theorem can be stated after defining some additional symbolism. Let s be any set of points in the x,y plane having a defined area. The area of s is denoted A[s], and the compliment of s (all points in the plane not in s) is denoted s*. For any v≥0, define

$$S(v) \equiv \textit{the set of points } (x, y) \textit{ satisfying } \tau(x, y) > v.$$

The theorem states (the proof is omitted for brevity) that

$$\int_s G(\tau(x, y))\, dxdy = G(0)\, A[s \cap S*(0)] - \int_0^\infty G(v) \frac{dA[s \cap S(v)]}{dv}\, dv$$

for any point set s and any function G such that the integrals exist. In particular, if G(0)=0, we can let s be the entire x,y plane to get

$$\int G(\tau(x, y))\, dxdy = -\int_0^\infty G(v) \frac{dF(v)}{dv}\, dv \quad \textit{if } G(0) = 0$$

where the integral on the left integrates over the entire x,y plane, and we used A[s∩S(v)]=A[S(v)]=F(v). The above equation can be expressed in terms of σ_{hi} by using (A3) and changing variables in the integral on the right to get

$$\int G(\tau(x, y))\, dxdy = \int_0^\infty G(\frac{Q_c}{a\, L}) \frac{d\sigma_{hi}(L)}{dL}\, dL \quad \textit{if } G(0) = 0. \qquad (A4)$$

A special case is given by G(ξ)=ξ. The integral on the left becomes the integral of τ(x,y) on the x,y plane, which, according to (A2), is the volume integral of Ω. The result is

$$\int \Omega(x, y, z)\, dxdydz = \frac{Q_c}{a} \int_0^\infty \frac{1}{L} \frac{d\sigma_{hi}(L)}{dL}\, dL. \qquad (A5)$$

Note that a change in the device orientation will rotate the function Ω, but this does not change the volume integral on the left side of (A5). This implies that the right side has the same value whether σ_{hi} is the normal-incident cross section or the directional cross section for some other direction.

Figure Captions

Fig.1: Heavy-ion SEL cross section for the HM65162 SRAM produced in 1985. Data (points) are from Levinson *et al.* [5]. The curve is from (7) using σ_0=0.116 cm^2, $L_{1/e}$=28.3 MeV-cm^2/mg.

Fig.2: Heavy-ion SEL cross sections for the AMD K-5 microprocessor. Data (points) are from internal memos, but the two highest points are very crude estimates. The curve is a hand sketch.

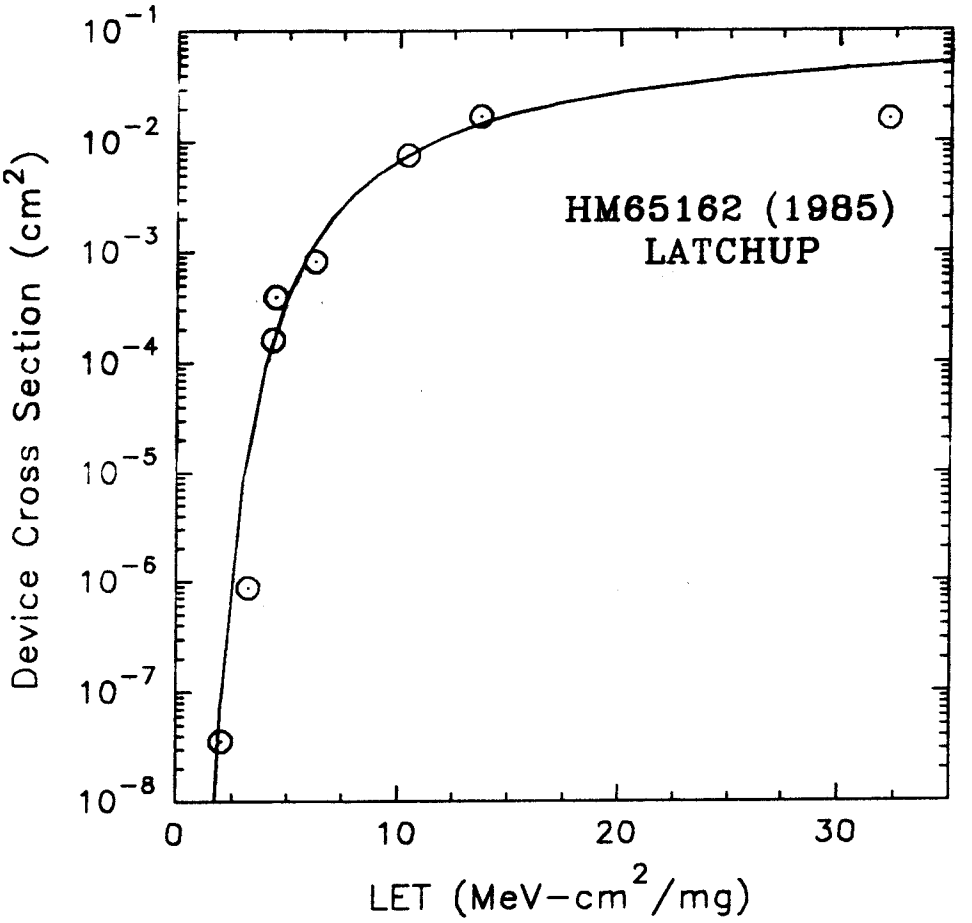

Fig. 1: Heavy-ion SEL cross section for the HM65162 SRAM produced in 1985. Data (points) are from Levinson *et al.* [5]. The curve is from (7) using σ_0=0.116 cm^2, $L_{1/e}$=28.3 MeV-cm^2/mg.

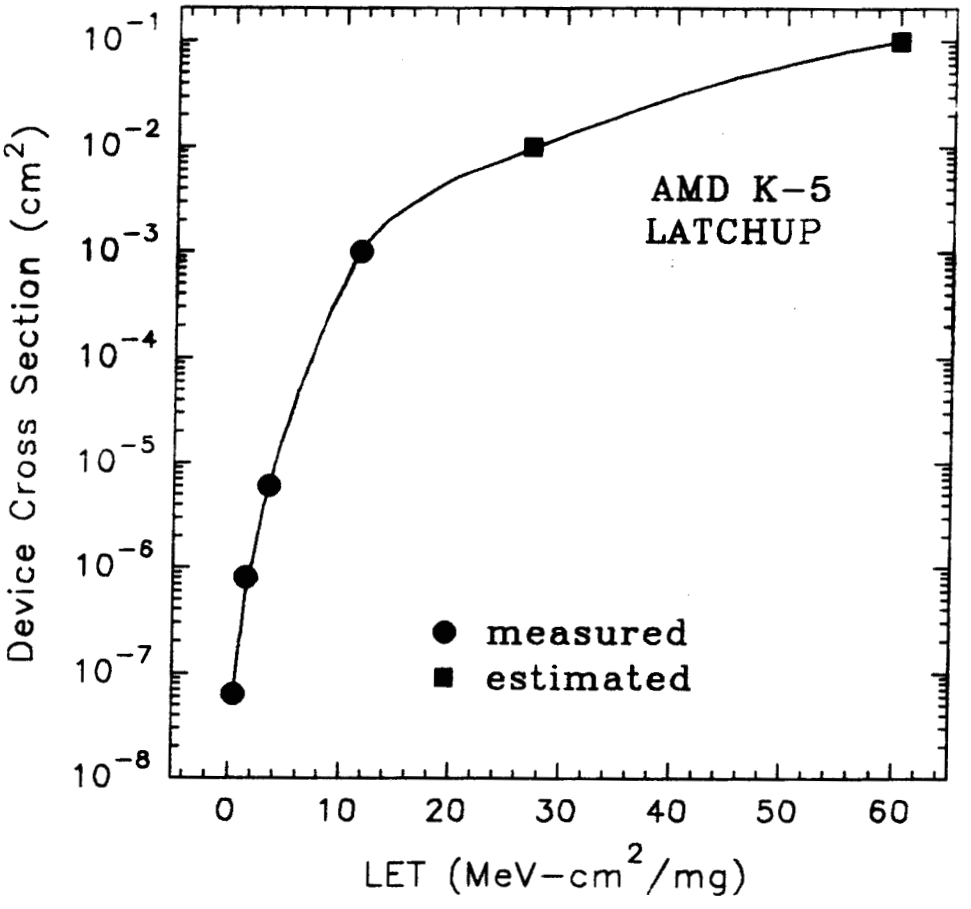

Fig.2: Heavy-ion SEL cross sections for the AMD K-5 microprocessor. Data (points) are from internal memos, but the two highest points are very crude estimates. The curve is a hand sketch.